Self-assembly and crystallization of double crystalline aliphatic thermoplastic biopolyurethane and its nucleation with cellulose nanocrystals

Borja Fernández-d'Arlas[1*], Ana Gabriella Arteaga,[2] Ainara Saralegi,[3,4] Maria Ángeles Corcuera,[3] Arantxa Eceiza,[3] Alejandro J. Müller,[2,5]

[1]NanoBioTechnology Group, CIC NanoGUNE, Avenida de Tolosa 1, 20018 Donostia-San Sebastián, Spain

*e-mail: borja.fernandezdarlas@ehu.es; telf.: (+34)685799709

[2]POLYMAT and Polymer Science and Technology Department, Faculty of Chemistry, University of the Basque Country UPV/EHU, Paseo Manuel Lardizábal 3, 20018, Donostia-San Sebastián, Spain

[3]Grupo"Materiales+Tecnologías" (GMT), Departamento de Ingeniería Química y del Medio Ambiente, Escuela Politécnica.Universidad del País Vasco/Euskal Herriko Unibertsitatea (UPV/EHU), Pza. Europa 1, 20018 Donostia-San Sebastián, Spain

[4]Departamento de Ingeniería Química y del Medio Ambiente, Escuela de Ingeniería de Vitoria-Gasteiz. Universidad del País Vasco/Euskal Herriko Unibertsitatea (UPV/EHU), Calle Nieves Cano 12, 01006 Vitoria-Gasteiz, Spain

[5]IKERBASQUE, Basque Foundation for Science, Bilbao, Spain

Abstract

An aliphatic segmented thermoplastic biopolyurethane (STPU), based on aliphatic hexamethylene diisocyanate (HDI) and 1,3 propanediol (1,3PD) as urethane rich phase and a poly(sebacate) as a macrodiol phase, with ~50 wt% of renewable carbon content, was synthetized and mixed with cellulose nanocrystals (CNC) to develop new bionanocomposites. The phase behaviour of the STPU and derived bionanocomposites was analysed with a variety of techniques which include differential scanning calorimetry (DSC), isothermal crystallization, X-ray scattering and atomic force microscopy (AFM). The Isothermal crystallization of the STPU matrix allowed fitting to the Lauritzen-Hofmann model and calculation of the overall crystallization constant, K_g^{τ}. Further dynamic thermal analysis by X-ray scattering and DSC allowed the determination of the impact of CNC on the morphology and nucleation of the urethane rich phase. Self-nucleation experiments with the STPU matrix allowed quantification of the nucleation effect of the CNC.

1. Introduction

Thermoplastic polyurethanes (TPU) are formed by the polycondensation of a bifunctional diisocyanate with one or various bifunctional glycols, either in one step or in sequential reactions, to improve segmentation leading to segmented TPU (or STPU). Polyurethanes based on aliphatic hexamethylene diisocyanate (HDI) were first reported in the 30-40s from the past century [1]. TPUs can be considered copolymers with the generic structure of –([D-G]$_x$-*b*-(D-M))-, where D represents the structure of the diisocyanate, G the structure of the glycol and M the structure of the macrodiol.

Due to the versatility of composition design and block disposition, TPU copolymers have potential for application in numerous sectors. TPUs based on aliphatic HDI are interesting for a range of applications in biomedicine, since their degradation does not lead to toxic aromatic amines as in the case of conventional aromatic based polyurethanes [2]. In addition to the pressure of finding new bioformulation of TPUs for their use *in-vivo* or in the biomedical field, there is also a motivation to pursue sustainable formulations that do not account for environmental damage [3,4]. In this sense, the use of macrodiols and glycols from renewable origin in TPU formulation might increase the portion of carbon from renewable sources considerably.

Polysebacates derived from castor (*Ricinus communis*) oil are being considered as an alternative to macrodiols such as polyesters or polyethers derived from mineral oil. These types of polyesters, in addition, tend to form semicrystalline phases what is interesting for shape-memory applications, among others. On the other hand, as has been previously shown, the use of propanediol (PD) derived from corn yields TPUs with similar performance to those analogs that include oil-derived PD [5]. In this work, we analyzed the self-assembly at the nanoscale, and the crystallization of the TPU synthesized with a poly(butylen)sebacate and PD as macrodiol and chain extender, respectively. As the diisocyanate linker, HDI was employed. In addition, cellulose nanocrystals (CNC), envisioned as very interesting materials for bioplastics reinforcement [6], were used to prepare bionanocomposites. In addition, the impact on the STPU self-assembly, nucleation, and crystallization was analyzed. The STPUs and derived bionanocomposites were analyzed by isothermal and non-isothermal differential scanning calorimetry (DSC), atomic force microscopy (AFM), and via wide (WAXS) and small (SAXS) scattering x-ray diffraction.

2. Experimental

2.1.Materials

The polyurethanes were synthesized from 1,6-hexamethylene diisocyanate (HDI, Bayer) and 1,3-propanediol (PD, Quimidroga SA) as hard segment, and a castor oil derived difunctional polyester (poly(butylene sebacate) diol) as soft segment (Merquinsa, S.A, Spain). The average molecular weight of poly(butylene sebacate)glycol was estimated considering the hydroxyl number of the polyol (I_{OH} = 60 mg KOH/g), determined by backward titration, following ASTM D 4274-05 test method A [7]. Thereby, an average value of 1900 g/mol was obtained. Microcrystalline cellulose (MCC) as well as dimethylformamide (DMF, >99.8%) and sulphuric acid (>98%), were supplied by Sigma Aldrich.

2.2.Preparation of Cellulose nanocrystals (CNC)

CNCs were extracted from MCC via acid treatment with sulphuric acid to remove amorphous and paracrystalline regions of cellulose, leaving intact only highly crystalline regions. Detailed procedure can be found elsewhere [6]. TEM and AFM analysis of CNC determined that the width and length of the fibers are 8 ± 1 nm and 152 ± 21 nm, respectively.

2.3.Synthesis of aliphatic thermoplastic biopolyurethane

The segmented thermoplastic polyurethane (STPU) was synthesized via two-stage route to promote block segmentation. In a first step, the hydroxyl terminated macrodiol based on poly(butylene sebacate)diol reacted with an excess of HDI at 90 ºC for 5h. The chain extender, PD, was added stoichiometrically, and after homogenization, the viscous liquid was poured into a Teflon-coated metal mould and reaction completed under pressure at 100 ºC for 10 h. Finally, samples were left cooling until room temperature before demoulded. These types of thermoplastics were previously characterized [8]. The molecular weight of the TPU matrix (STPU46) is in the range of 40000-50000 g/mol with a IP of ~2.6, as measured by gel permeation chromatography, based on polystyrene standards. In this work, a STPU with 46 wt% of urethane rich segment (HDI+PD) was used for the analysis of its self-assembly and crystallization in the presence of

CNCs. This material was achieved by a sequential reaction of HDI with the macrodiol in a ratio HDI:macrodiol = 7:1, and a second chain extension step of the resulting prepolymer with PD with a mole ratio of HDI:PD = 7:6. This TPU was named STPU46.

2.4.Preparation of biopolyurethane/cellulose nanocrystals bionanocomposites

CNCs were mixed with the STPU in dimethylformamide (DMF). A detailed description of the bionanocomposites preparation is explained elsewhere [6]. Briefly, after sonication of STPU and CNCs solutions, these were cast onto Teflon molds and dried in an oven under controlled pressure and temperature conditions. Composites with different loads (1, 3, 5 and 10 wt%) of CNCs were obtained and were named indicating the wt% of CNC added to the STPU46, i.e., STPU46-1, STPU46-3, STPU46-5 and STPU46-10. The bionanocomposites synthesized here, consisted thus on ~50 wt% of renewable carbon.

2.5.Thermal characterization of biopolyurethane

Biopolyurethane was characterized both using isothermal crystallization and non-isothermal DSC runs. The equipment used was a Perkin Elmer DSC 8500. The equipment was previously calibrated with indium and tin standards. Samples of ~3 mg were encapsulated in Al capsules for analysis. The non-isothermal runs were conducted as follows:

1. Heating at 20 ºC/min from 25 ºC to 180 ºC.
2. Isothermal step at 180 ºC for 3 min.
3. Cooling at 20 ºC/min from 180 ºC to -20 ºC.
4. Isothermal step at -20 ºC for 1 min.
5. Heating from -20 ºC to 180 ºC at 20 ºC/min.

The isothermal crystallization studies of STPU46 were conducted after the determination of the minimum $T_{c,min}$ (see appendix), as recommended by Lorenzo et al. [9]. Crystallization temperatures (Tc), above $T_{c,min}$, were selected, and the following thermal treatments were applied:

1. Heating from 25 ºC to 180 ºC at 20 ºC/min.
2. Isothermal step at 180 ºC for 3 min (thermal history erasure).
3. Cooling from 180 ºC to selected T_c at 120 ºC/min.
4. Isothermal step at T_c for a specific time.
5. Heating from T_c to 180 ºC at 20 ºC/min.

6. Repetition of steps 2-5 at different T_c.

The self-nucleation experiments were performed with STPU46 for analyzing the crystallization of HDI-PD segments. The study of different self-nucleation temperatures, T_s, and the Domain borders were discerned according to the method developed by Müller et al. [10], with the following temperature program:

1. Isothermal step at 180 ºC for 3 min (thermal history erasure).
2. Cooling from 180 ºC to -20 ºC at 20 ºC/min.
3. Isothermal step at -20 ºC for 1 min.
4. Heating from -20 ºC to selected T_s at 20 ºC/min.
5. Isothermal step at T_s for 5 min (self nucleation).
6. Cooling from T_s to -20 ºC at 20 ºC/min.
7. Isothermal step at -20 ºC for 1 min.
8. Heating from -20 ºC/min to 180 ºC at 20 ºC.
9. Repetition of steps 1-8 for selected T_s.

2.6. X-ray analysis of STPU46

Wide angle scattering data was acquired in a Bruker D8 Advance with a wavelength of $\lambda = 1.54$ Å in the range of 2θ of 5-30º. Samples were heated and cooled in an Anton Paar TTK450 chamber in vacuum. X-ray patterns were recorded after dynamic crystallization by slowly cooling from 160 ºC to -20 ºC.

Small angle scattering data was required in a Rigaku 3-pinhole PSAXS-L operating at 0.88 mA, with CuK (alpha) photons with a $\lambda = 1.542$ Å. The scattering was recorded in the range of $0.01 < Q < 0.15$ Å^{-1}. The thermal treatment was similar to that applied in WAXS analysis.

2.7. Atomic Force Microscopy of crystallized polyurethane

A solution of STPU46 in a mixture of tetrahydrofuran (THF): dimethylformamide (DMF) (THF:DMF = 3:1) was prepared at a concentration of 0.1 wt%/v by swelling at room temperature (RT) for 14 h and then by magnetic stirring at 60 ºC for 2h. Then one drop was cast into mica by spin-coating and the sample dried for 48h under vacuum at RT. In order to crystallize the STPU46 under a defined structure, oriented by DSC results, the following thermal treatment was applied

on a heating plate: (1) Sample was heated to 180 ºC and kept at this temperature for 3 min; (2) the sample was then rapidly transferred to another plate at 131 ºC and crystallized for 14 h.
Images of the crystallized sample were acquired at RT and 80 ºC in a Nanoscope IV Digital Instruments (Veeco) with a E-Scanner and using silicon tips.

3. Results and discussion

3.1. STPU and bionanocomposites structure as evidenced by thermal analysis (DSC)

The synthesized STPU is composed of a semicrystalline macrodiol based on vegetal oil-derived poly(butylen)sebacate. The urethane rich phase is composed of 1,3-propanodiol, which today is derived from corn, and aliphatic 1,6-hexamethylene diisocyanate derived from oil cracking. Therefore, a combination of these monomers leads to STPU polymer (Figure 1) with high renewable content. In comparison to typical elastomers based on TPU, which are formulated with macrodiols that form rubbery phases at ambient temperatures (T_{am}) above crystallization, in case of semicrystalline macrodiols, and glass transition temperatures ($T_{am} >> T_c > T_g$), in the present case the poly(butylen)sebacate forms a semicrystalline phase with a melting temperature above ambient temperature ($T_c > T_{am}$). This has important consequences on STPU morphology and properties, and the research and development of these types of STPU is attractive for applications requiring materials with high shape fixity and memory, such as for example, future implants for tissue regeneration or grafts for veins restitution. If the ambient temperature approaches the macrodiol crystallization (T_c) or melting temperatures (T_m) in a shape fixed material the morphology might be substantially modified towards a pre-determined shape [8,**¡Error! Marcador no definido.**].

Double crystalline polymers are interesting for shape-memory materials, since while the low temperature phase triggers the shape variation, the high temperature crystalline phase holds the material and avoids melting and flowing. As can be seen in Figure 2, the melting temperature of the macrodiol phase in the pure STPU46 matrix (also in the derived bionanocomposites) is in the range of 46-49 ºC. This value is considerably lower to that of the pure macrodiol melting temperature (T_m ~ 71 ºC). On the other hand, the high melting temperature HDI-PD (herein after called ‘hard segment’, HS) semicrystalline phase melts in the range of 151-154 ºC (what can be compared with the value for the peak of the pure HDI-PD melting curve, i.e., T_m ~ 165 ºC). This bimodal melting trace is similar to that reported for poly(tetramethylene)glycol HDI based

polyurethanes [4]. Figure 2 shows that in the second heating scan, the SS phase melting temperature is lower than in the first run, something that can be explained by an annealing process of the macrodiol at samples storage temperature (i.e., $T_a \sim T_{amb}$) leading to thicker lamellae that melt at higher temperatures.

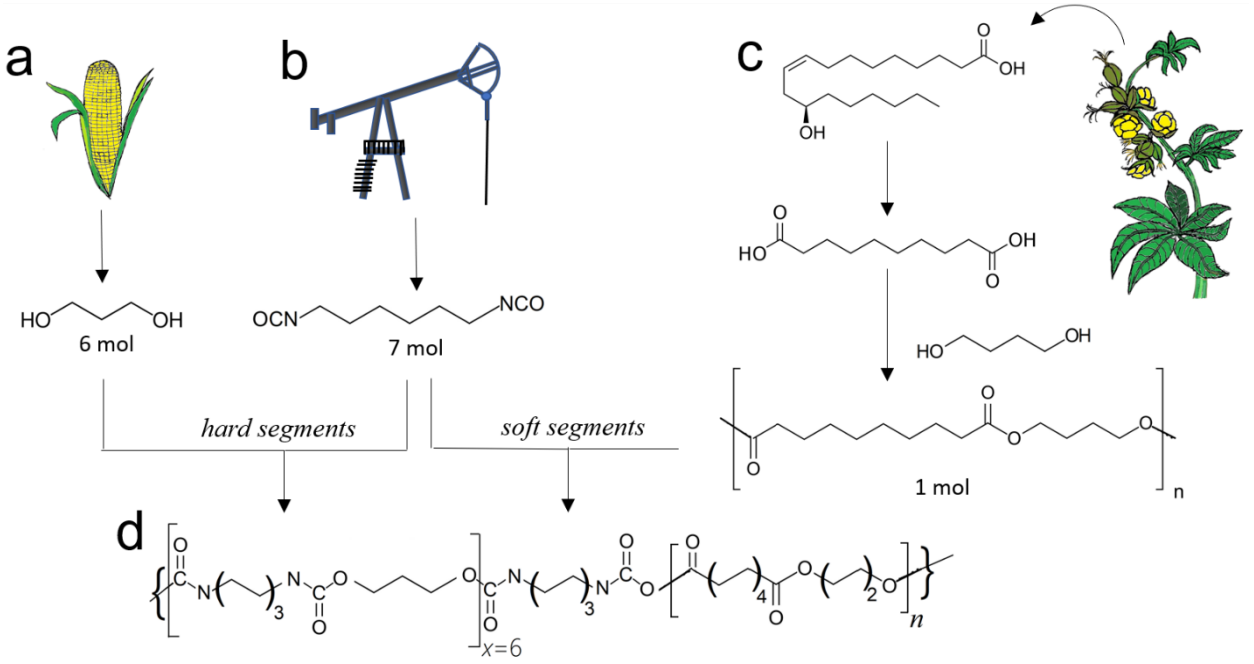

Figure 1. Origin and relationship between the chemicals used to synthesize the STPU46 matrix of the present study. a) 1,3 propanodiol (PD) is a glycol that can be derived from corn. b) The diisocyanate 1,6 hexamethylen diisocyanate (HDI) is derived from ethane extracted from oil cracking. c) The poly(butilen)sebacate macrodiol used as main component of the 'soft segments' is derived from ricinoleic acid, extracted from *Ricinus Communis* (Castor) seed oil, after polymerization of obtained succinic acid with 1,4-butanediol. d) Structure of the STPU46 biopolyurethane thermoplastic.

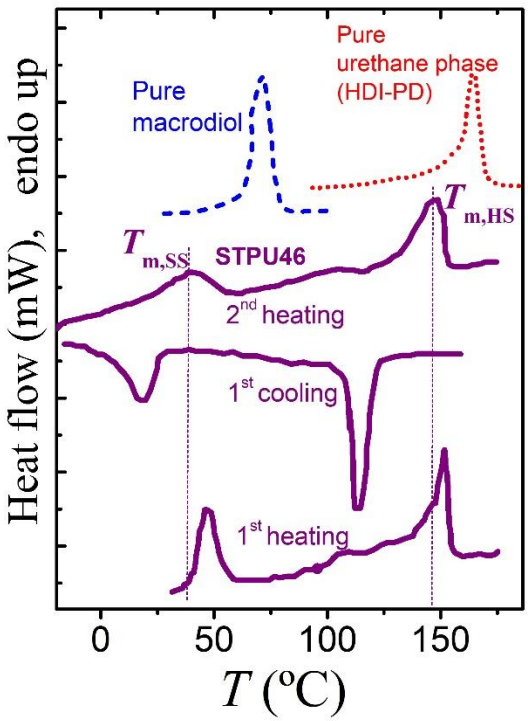

Figure 2. Dynamic thermal analysis of the STPU46 matrix indicating the 1st heating, cooling and 2nd heating steps and the melting temperature of the soft and hard phase ($T_{m,SS}$ and $T_{m,HS}$, respectively) along with the melting endotherms of the pure macrodiol and urethane phase (HDI-PD) [8].

3.2. X-Ray analysis of the bimodal melting process

Analysis of the WAXS at different temperatures allows identifying the double crystalline structure of the materials. Figures 3a and 3b show the WAXS and SAXS scattering patterns of the biopolyurethane matrix STPU46 at three chosen temperatures in which both phases are semi-crystalline (-20 ºC), one melted and the other crystallized (80 ºC) and both molten (180 ºC). From -20 to 80 ºC, it is seen that the signals at 6.1 and 21.5º (marked with a vertical line) disappear. Thus, these peaks might be ascribed to the poly(butilen)sebacate macrodiol crystals, which, as we showed above in the DSC study, melt in the range of 42-48 ºC. At 80 ºC the peak at 20.0º (d = 4.4 Å) is prominent and remains along with peaks at 6.8º (d = 13.0 Å) and 24.3º (d = 3.7 Å). These reflections are in the range with interplanar distances found for other HDI based aliphatic urethane phases [11]. At 180 ºC only an amorphous halo centered at 2θ = 19º is observed and is typical for thermoplastic polyurethanes in the molten state [12,13,14]. In Figure 3b a progressive increase of the interdomain distance d^* with temperature is observed: from d^* = 11 nm at -20 ºC to d^* = 14

nm at 80 ºC, disappearing at 180 ºC due to complete melting. A description of the physical process as described by SAXS results is depicted in Figure 3c.

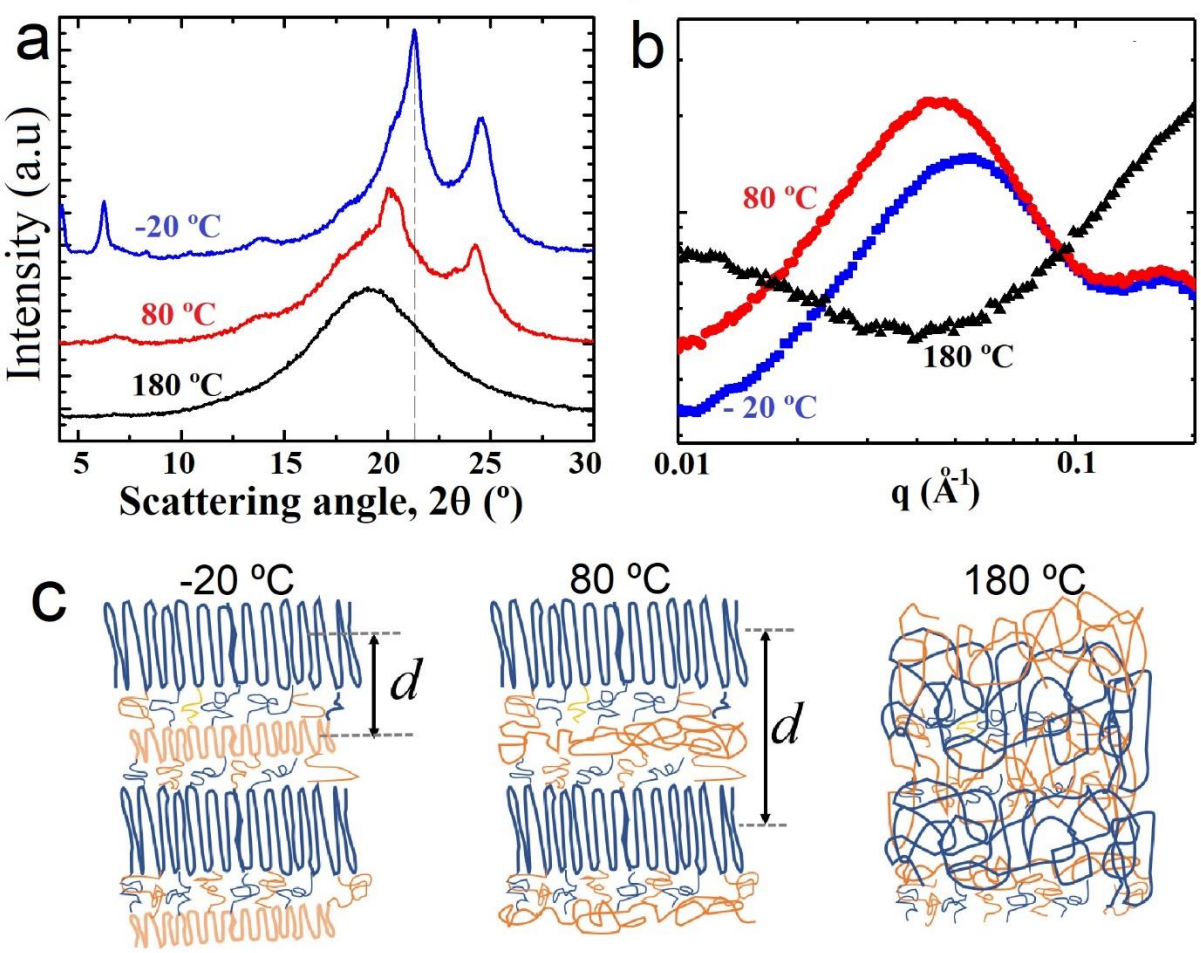

Figure 3. X-ray diffraction experiments at different temperatures. a) WAXS. b) Lorentz corrected (Iq^2) SAXS spectra. c) Scheme that interprets X-ray results. HDI-PD crystals are depicted in blue while poly(butilen)sebacate crystals are in orange.

3.3. Atomic force microscopy visualization of the bicrystalline morphology

Figure 4a shows the spherulitic morphology of a crystalized (T_c = 131 ºC) STPU46 sample. Higher magnification images (Figure 4b) reveal that the spherulites are composed by radial lamellae which in turns, are also composed by smaller lamellae (i.e., primary lamellae). Observation of the lamelar morphology by AFM has been previously reported for TPUs with varied primary structure [15,16]. The sizes of the large secondary lamella in Figure 4b are in the range 170-210 nm. On the other

hand, the primary lamellae (observed in the detail of Figure 4b) have sizes in the range 55-75 nm. This range fits with data predicted by the Gibbs-Thomson equation [17]:

$$l_c = \frac{2\sigma_e T_m^0}{\Delta H_v (T_m^0 - T_m)} \quad (1)$$

Where σ_e, T_m^0 and ΔH_v are the lamellar end surface free energy, the melting temperature at the thermodynamic equilibrium and the molar volume melting enthalpy, respectively. Being σ_e:

$$\sigma_e = \frac{k\, K_g^t}{0.2\, T_m^0\, b_o \sqrt{a_0 b_0}} \quad (2)$$

the lamellar thickness, l_c (Figure 4d), might be estimated by approximating the cell parameters, a_0 and b_0 as $a_0 \sim b_0 \sim 4.5$ Å, using the overall kinetic constant, $K_g^{\tau} = 1.2 \times 10^5$ K^2 (calculated below in the isothermal experiments), $T_m^0 \sim T_{m,end} = 160$ ºC (see Figure 2), $\Delta H_v \sim 81$ J/g x 1.2 g/cm^3, T_m =149.5 ºC (for a $T_c = 131.5$ ºC). The value is thus obtained by combining eqs. (1) and (2) are of l_c = 65 nm, which lays in the range of lamellar sizes measured with AFM for the primary lamellae. Progressively heating a crystallized sample under the AFM tip shows that the spherulitic texture is mainly sustained and driven by the urethane rich phase, HDI-PD, which only melts at temperatures above 150 ºC. At 80 ºC, well above the melting temperature of the poly(butylen)sebacate macrodiol, the spherulitic texture is well maintained (Figure 4c and 4e). As in the case of TPUs based on HDI-,1,4 butanediol segments [18] the lamellar morphology definition is thus ascribed to the association of HDI-PD segments into lamellar domains.

3.4. Isothermal crystallization of the STPU46 matrix

Crystallization under isothermal conditions was conducted at different temperatures. These experiments allow interpreting the impact of composition on lamellar formation. Studying the isothermal crystallization by DSC means usually provides an idea of the overall crystallization rate, this is, a combination of the primary nucleation and the secondary nucleation rates. Figure 5a shows heat flow curves obtained by isothermal crystallization in the DSC, performed at different crystallization temperatures, T_c. From the heat release curve, the overall crystallization rate can be estimated. The Lauritzen-Hofmann model can be used here to calculate the overall crystallization constant, K_g^{τ}, by considering the half crystallization rates ($1/\tau_{50\%}$) proportional to the growth rates [19]:

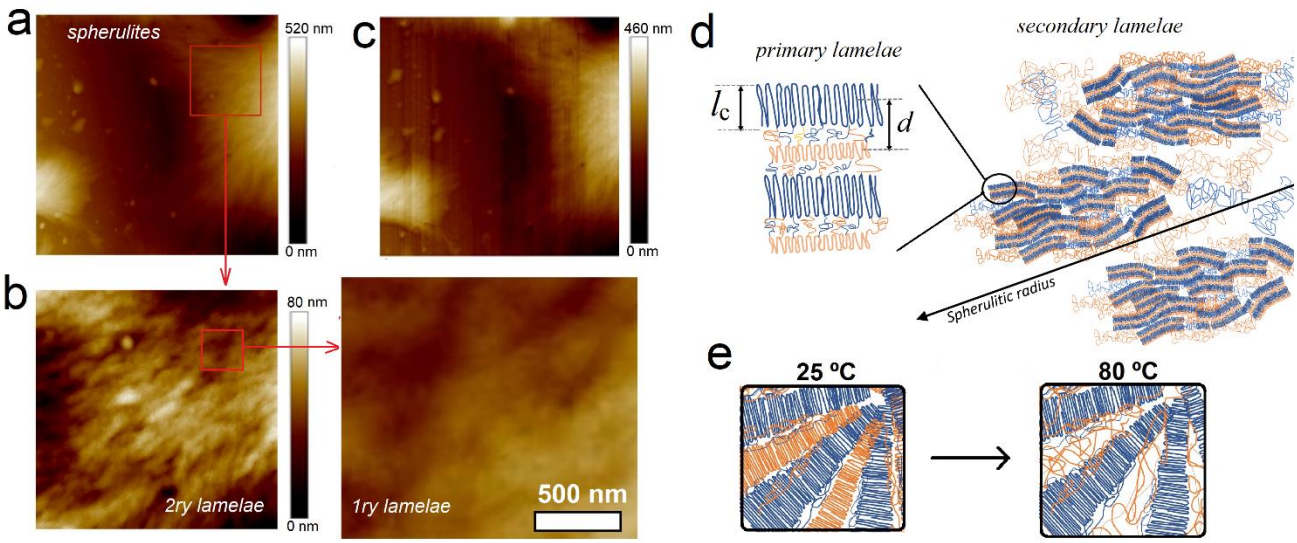

Figure 4. Morphology of crystallized STPU46 at different temperatures as observed by AFM. A) 15 x 15 μm^2 image at RT. b) Lamellae seen at a magnified image of 6 x 6 μm^2. c) 15 x 15 μm^2 image at 80 ºC. d) Scheme of the spherulitic morphology composed on primary lamellae assembled into radial secondary lamella. e) Melting of the poly(butylen)sebacate crystals within spherulitic morphology.

$$\frac{1}{\tau_{50\%}} = \frac{1}{\tau^0_{50\%}} exp\left[\frac{-U^*}{R(T_c - T_\alpha)}\right] . \left[\frac{-K_g^\tau}{f \cdot T_c (T_m^0 - T_c)}\right] \quad (3)$$

Where T_α is a temperature where no long-ranged molecular motion occurs, taken as $T_\alpha \sim T_g$-30ºC, f a temperature correction factor defined as $f = 2T_c/(T_c+T_m^0)$, and U^*, the activation energy required to displace the macromolecules to the crystallizing front, taken as 1500 cal·mol^{-1} or 6280 J·mol^{-1}. Here the T_m^0 value was approximated to the end temperature of the melting endotherm, $T_m^0 \sim T_{m,end}$ = 160 ºC (see Figure 2). The glass transition temperature, T_g was taken as $T_g \sim 90$ ºC. A plot of $\ln(1/\tau_{50\%}) + U^*/R(T_c - T_a)$ vs. $1/f \cdot T_c(T_m^o - T_c)$ yields a straight tendency whose fitting allows calculating K_g^τ from the slope (Figure 5b). This procedure yielded a value of $K_g^\tau = 1.2 \cdot 10^5$ K^2. This value is significantly smaller than those obtained for TPUs based on MDI-BD urethane rich segments, with different macrodiols and similar portion of MDI-BD segments [20]. In view of K_g^τ, as a constant proportional to the energy barrier required for the polymer chains to nucleate (primary nucleation) and grow (secondary nucleation) and considering the more voluminous nature of MDI-BD than HDI-PD segments, these findings have plenty of sense.

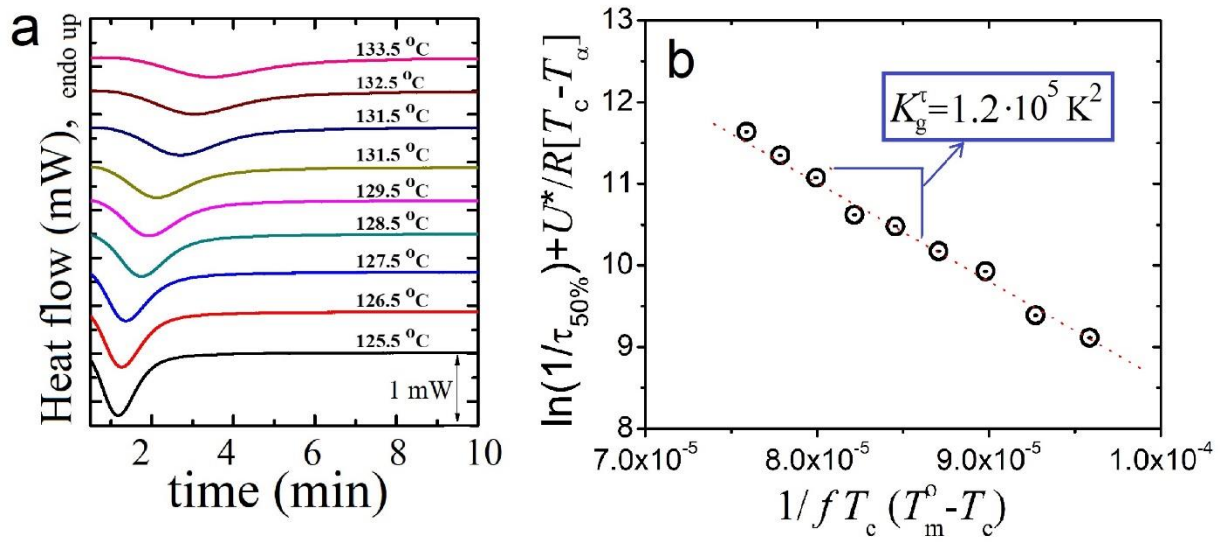

Figure 5. Calorimetric DSC analysis of the crystallization rate of STPU46. a) Isothermal traces of the heat flow over time at the indicated crystallization temperatures. b) Determination of the overall crystallization rate by application of the Lauritzen-Hoffman theory.

3.5.Impact of CNC on the morphology and non-isothermal thermal behaviour.

As has been previously shown, CNC increases STPU46 elastic modulus from 199 MPa (neat TPU) to 359 MPa (filled with 10 wt% CNC), has moderate impact on yield and tensile strength, and diminishes the extensibility of these TPU materials under strain [6]. The subsequent analysis presented here has the intention to further provide insights on the CNC impact on STPU46 matrix bi-crystalline morphology and on the ulterior structure-properties relationships. Figure 6 presents the heating and cooling curves of the STPU46 matrix and derived composites with CNCs. In Figure 6b, it is seen how the crystallization temperature of the HS (peak) is slightly increased with the addition of CNCs. This is ascribed to a nucleation effect of the CNCs over the HDI-PD urethane rich segment, presumably promoted by hydrogen bonding between the urethane groups and the cellulose hydroxyls. In contrast, CNCs do not appear to have an effect on the SS crystallization or melting temperature. Melting and crystallization temperatures along with the melting and crystallization enthalpies are gathered at Tables 1, 2 and 3. As seen in Tables 1-3, whereas the CNC increases the crystallization temperature by about 5 ºC, it appears to not have impact on the melting temperature. As seen in Tables 1-3, the crystallization and melting enthalpies of the hard and soft phases appear to diminish with the incorporation of CNCs. This also occurs in absolute

terms, when the heat is normalized with the fraction of each of the considered crystallizing phase. This might be explained by a reduced mobility induced by CNCs, which, in addition, interact with the hard HDI-PD segments, as observed during the cooling scans as a nucleating effect. However, at high CNC contents, this behaviour is less pronounced, because above the percolation threshold (~3 wt%) CNCs tent to agglomerate [6,21], and thereby, the interaction between CNCs and the matrix is reduced.

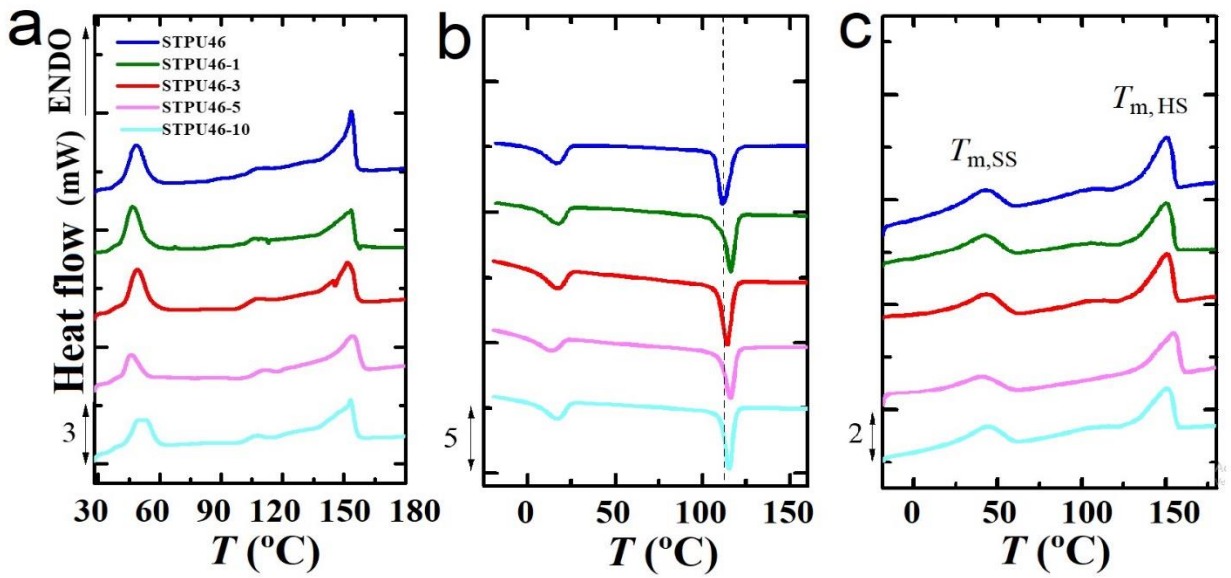

Figure 6. Non-isothermal analysis of the bionanocomposites. a) Heating curves of materials after synthesis and annealing at RT. b) Cooling curves from the molten state. c) Second heating curves immediately after the cooling step.

Table 1. Melting temperature peaks and respective enthalpies of the soft and hard phases in the pure STPU46 matrix and composites with 1, 3, 5 y 10 wt% CNCs at the first heating.

Sample	Soft phase			Hard phase		
	T_m *SS* (ºC)	ΔH_m *SS* (J/gPU)	*ΔH_m *SS* (J/gSS)	T_m *HS* (ºC)	ΔH_m *HS* (J/gPU)	*ΔH_m *HS* (J/gHS)
STPU46	48.7	39	87	153.8	85	157
STPU46-1	46.7	40	92	153.4	81	151
STPU46-3	49.0	34	80	151.6	83	158
STPU46-5	46.0	16	38	154.1	74	144
STPU46-10	49.6	26	66	153.2	68	140

*Normalized melting enthalpies respect to the weight fraction of the specific phase (SS or HS) in the bionanocomposite.

Table 2. Crystallization temperature peaks and respective enthalpies of the soft and hard phases in the pure STPU46 matrix and composites with 1, 3, 5 y 10 wt% CNCs at the cooling step.

Sample	Soft phase			Hard phase		
	T_c *SS* (ºC)	ΔH_c *SS* (J/gPU)	*ΔH_c *SS* (J/gSS)	T_c *HS* (ºC)	ΔH_c *HS* (J/gPU)	*ΔH_c *HS* (J/gHS)
STPU46	16.9	-33	-75	111.5	-81	-150
STPU46-1	17.9	-34	-78	116.2	-70	131
STPU46-3	17.1	-29	-68	115.0	-71	-135
STPU46-5	13.6	-24	-57	116.1	-60	-117
STPU46-10	17.0	-29	-73	115.3	-52	-107

*Normalized crystallization enthalpies respect to the weight fraction of the specific phase (SS or HS) in the bionanocomposite.

Table 3. Melting temperature peaks and respective enthalpies of the soft and hard phases in the pure STPU46 matrix and composites with 1, 3, 5 y 10 wt% CNCs at the second heating.

Sample	Soft phase			Hard phase		
	T_m *SS* (ºC)	ΔH_m *SS* (J/gPU)	*ΔH_m *SS* (J/gSS)	T_m *HS* (ºC)	ΔH_m *HS* (J/gPU)	*ΔH_m *HS* (J/gHS)
STPU46	42.1	37	84	150.7	81	150
STPU46-1	43.0	37	85	150.7	74	138
STPU46-3	43.3	35	82	150.8	78	149
STPU46-5	40.2	27	64	154.5	63	123
STPU46-10	43.8	27	68	151.0	70	144

*Normalized melting enthalpies respect to the weight fraction of the specific phase (SS or HS) in the bionanocomposite.

3.6. Isothermal crystallization of bionanocomposites

Analysis of the isothermal crystallization of the bionanocomposites with CNCs can provide information on the nucleating activity of the cellulose and its impact on the crystallization rate of the HS phase. Analysis of isothermal DSC curves of bionanocomposites similar to those presented previously for STPU46 provides half crystallization times, whose inverse is plotted in Figure 7a. From the data it is not possible to extract a direct consequence of the CNCs on the crystallization rate. The isothermal curves can be fitted to the Kolmogorov-Avrami model [22, 23, 24]. The procedure for an optimal fitting is described by Lorenzo et al. [9] This led to an excellent fitting of our data in the primary crystallization range (Figure 7b) providing information on the parameters of the model equation:

$$1 - \phi_c(t - t_0) = \exp[-K(t - t_0)^n] \quad (3)$$

where $\phi_c(t)$ is the crystalline relative volumetric fraction at a time t; K the overall crystallisation rate constant; t, the crystallisation time; t_0 the induction time and n the Avrami exponent. Conditions and fitting parameters to equation (3) are gathered in the Appendix. Figure 7c and 7d plot the Avrami exponent, n, and the normalized crystallization rate constant, $K^{1/n}$, for the STPU46 and derived bionanocomposites. The Avrami model presents an approximation to the overall crystallization process but does not provide details at the molecular level. Nevertheless, it provides information with respect to the nucleation event (sporadic or instantaneous) and on the dimensionality of the crystal growth (2D or 3D). Here, the Avrami index, n, appears to be higher in CNC nucleated composites than in pure STPU46. This is an unexpected result, and for example opposite to results found, under similar analysis, for MDI based TPUs in the presence of polyhedral oligomeric silsesquioxane (POSS) as nucleating agent [25]. On the other hand, the non-isothermal results indicate that CNCs can nucleate the material and the overall crystallization kinetics shown in Figure 7a shows that the overall crystallization kinetics is accelerated by the addition of CNC. Considering these results, one would expect the Avrami index to be reduced when CNCs are added to the matrix. A more in-depth study on the nucleation effect would be needed to understand this result, which is outside the scope of the present work.

As the T_c increases the n index progressively increases within the range n = 2.7-4.0. This is the opposite tendency found for MDI-BD based TPU when increasing T_c [20]. The trend found here corresponds to the normal behaviour where the nucleation varies from an almost instantaneous process at low temperatures to a more sporadic (higher n) at higher temperatures.

The evolution of $K^{1/n}$ with respect T_c is similar to the evolution of the half crystallization time, $1/\tau_{50\%}$ indicating that the Avrami model allows to predict qualitatively the crystallization of these materials up to about 50% conversion to the semi-crystalline state.

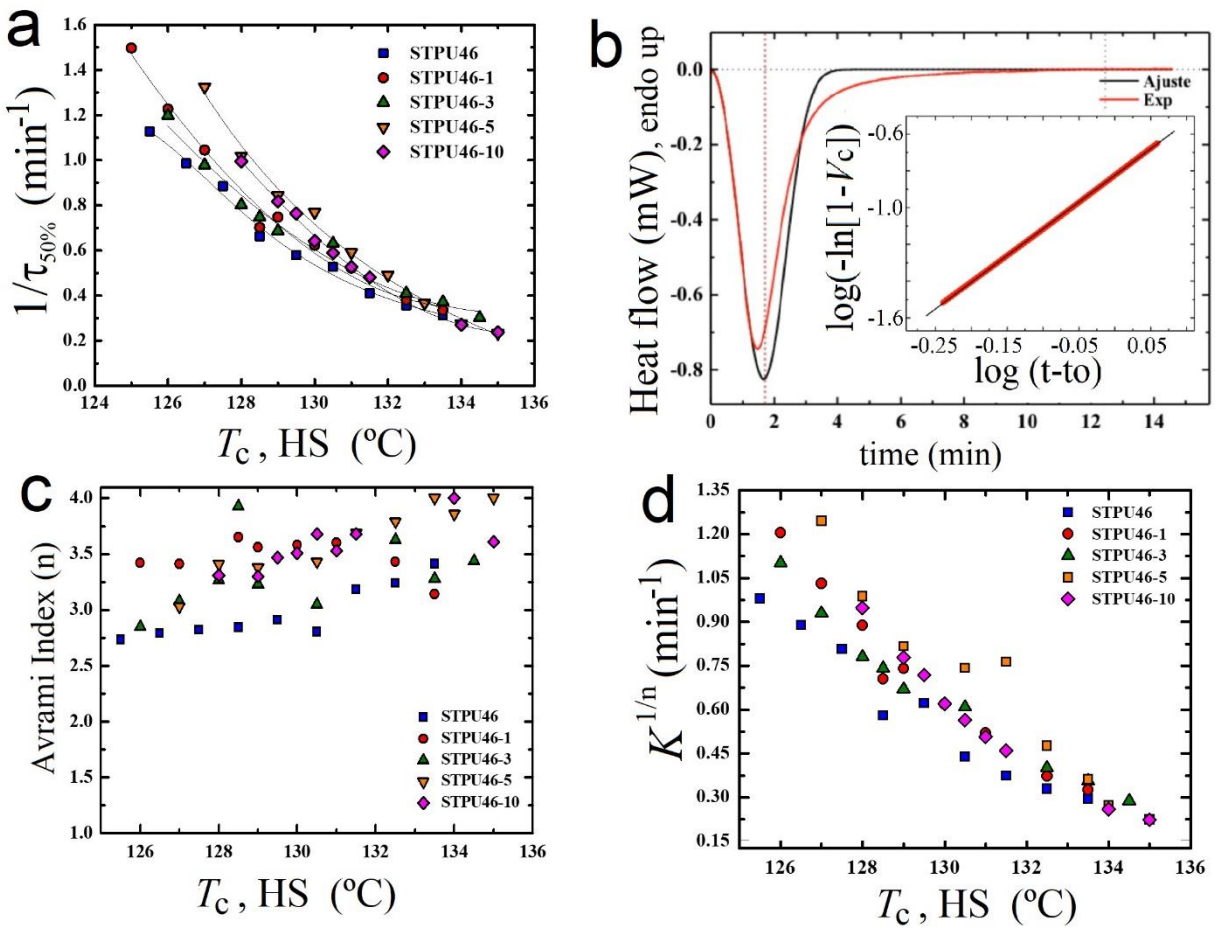

Figure 7. Isothermal crystallization of bionanocomposites. a) Inverse of the half crystallization times for different crystallization temperatures, T_c. b) Original heat flow curve for the STPU46 matrix along with the Avrami fitting obtained by the Plug-in developed by Lorenzo et al. [9]. c) Avrami indexes for the hard phase crystallization within bionanocomposites with different CNC content, as function of T_c d) Normalized Avrami pre-exponential constant K as function of T_c.

3.7. Self-nucleating activity of STPU46 and heterogeneous CNC nucleation of HS

Heterogeneous nucleation was widely studied by Fillon et al. and they proposed a manner for quantification of nucleation efficiency, based on the pure matrix self-nucleation activity [26]. The self-nucleation (SN) activity is highly dependent on polymers chemistry and has been widely studied by Müller et al. [27] for a variety of homopolymers and copolymers. The SN experiments allow determining the domains or temperature ranges over which the nucleation events are of heterogeneous nature (Domain I, *DI*), the range in which these occur over self-nuclei (Domain II, *DII*), and the range in which self-nucleation and crystal annealing of unmolten crystals happen simultaneously (Domain III, *DIII*).

Figure 8a shows the cooling curves from different tentative T_s, and Figure 8b shows subsequent heating scans. Cooling from *DI* develops a 'standard' morphology of a material cooled from the melt. Upon self-nucleation and cooling from *DII* the crystallization temperature is significantly increased due to the nucleating activity of self-nuclei. The border between *DI* and *DII* is identified thus in the temperature range of 158-160 ºC. The border between *DII* and *DIII* is identified as the temperature below which annealing appears as detected as a melting shoulder in subsequent heating. The curves cooled from 156 and 155 ºC are within *DII*, while those below 154 ºC are already at *DIII*. Figure 8c presents the data of STPU46 crystallization temperature, T_c (squares), superimposed to the standard melting curve where the domain borders are marked with vertical lines. It is seen how within *DII* the T_c increases by about 13 ºC.

It is important to note that the self-nucleation experiments performed here is specifically oriented to definition of the hard phase (HDI-PD segments). Studying the soft phase curves, it is seen that the soft segments are not affected by the morphology of the hard phase and segments and it its nucleated by these.

From data extracted from Figure 8c, it is possible to calculate the nucleating efficiency, *NE*, of a heterogeneous agent such as CNC, by using the equation introduced by Fillon *et al*. [23]:

$$NE\ (\%) = \frac{T_{C,NA} - T_C}{T_{C,Max} - T_C}\, x\ 100 \qquad (4)$$

where $T_{c,NA}$ represents the crystallizing temperature in the presence of nucleation agent (i.e., CNC), T_c the crystallization temperature of the neat polymer and $T_{c,Max}$ the maximum crystallization temperature achieved by self-nucleation at a T_s ideal. Table 4 gathers the data used for the

calculation of the NE and the results obtained. It is seen that the values fluctuate between 27 and 37 % suggesting that with 1 wt% of CNC the NE is saturated.

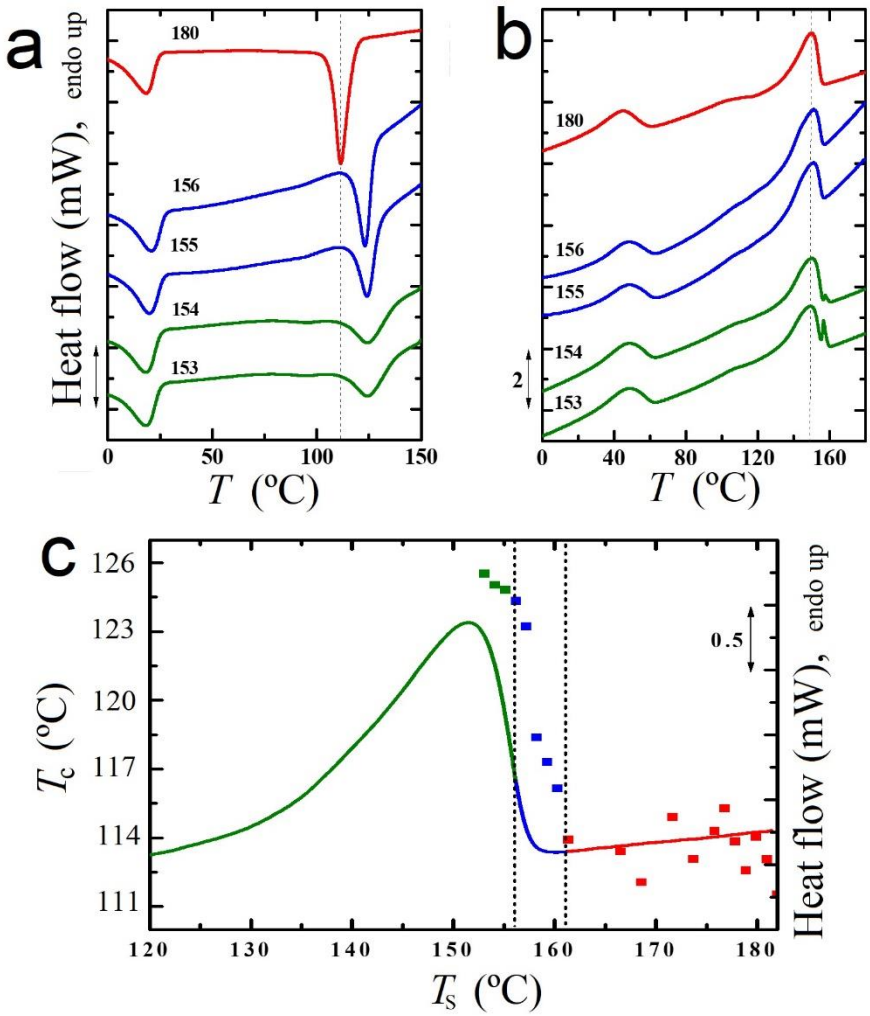

Figure 8. Self-nucleation of the STPU46 matrix. a) Cooling curves from indicated T_s. b) Subsequent heating curves after self-nucleation at indicated T_s. c) Crystallization temperatures of STPU46 after self-nucleation at different T_s, superimposed with the standard melting curve and domain borders.

Table 4. Data and results of the self-nucleation and heterogeneous nucleation of 1, 3, 5 y 10 wt% CNCs.

Sample	**Nucleating agent** / **CNC (%)**	***T_c*** **Pure polymer (ºC)**	***T_c NA*** **(ºC)**	***T_c máx.*** **(ºC)**	***NE*** **(%)**
STPU46	1	111.5	116.2	124.3	37
	3		115.0		27
	5		116.1		36
	10		115.3		30

4. Conclusions

Upon cooling from the melt, the neat STP46 biopolyurethane matrix exhibits a double crystalline morphology, as determined by DSC, X-ray diffraction, and AFM. Isothermal crystallization of the STPU and composites allowed estimation of the crystallization kinetics parameters. Non-isothermal thermal analysis and self-nucleation experiments by DSC allowed the determination of the nucleating efficiency of CNC over the hard phase composed by HDI-PD segments. The efficiency of nucleation of CNCs is low and restricted to the HDI-PD segments, and it saturated at 1 wt% of CNC.

Acknowledgments

A.Eceiza and A. Saralegi acknowledge funding from the University of the Basque Country (UPV/EHU) (GIU18/216 Research Group). Moreover, authors are grateful to the Macrobehavior-Mesostructure-Nanotechnology SGIker unit of the UPV/EHU. This work has received funding from the Basque Government through grant IT1309-19. BFD wants to acknowledge Prof. Raúl Pérez Jiménez from NanoGUNE and 'BioUPGRADE' European Commission Project.

REFERENCES

[1] O. Bayer. Das Di-Isocyanat-Polyadditionsverfahren (Polyurethane). Angew. Chem. A 59 (1947) 257-288.

[2] J.P. Santerre, K. Woodhouse, G. Laroche, R.S. Labow. Understanding the biodegradation of polyurethanes: From classical implants to tissue engineering materials. Biomaterials 26 (2005) 7457–7470.

[3] A. Tenorio-Alonso, M.C. Sánchez, J.M. Franco. A Review of the Sustainable Approaches in the Production of Bio-based Polyurethanes and Their Applications in the Adhesive Field. Journal of Polymers and the Environment (2020) 749–774.

[4] Z. Shen, L. Zheng, C. Li, G. Liu, Y. Xiao, S. Wu, J. Liu, B. Zhang. A comparison of non-isocyanate and HDI-based poly(ether urethane): Structure and properties. Polymer 175 (2019) 186–194.

[5] B.J. Rashmi, D. Rusu, K. Prashantha, M.F. Lacrampre, P. Krawczak. Development of bio-based thermoplastic polyurethanes formulations using corn-derived chain extender for reactive rotational molding. eXPRESS Polym. Lett. 10 (2013) 852–862.

[6] A. Saralegi, L. Rueda, M.D. Martin, A. Arbelaiz, A. Eceiza, M. Corcuera. From elastomeric to rigid polyurethane/cellulose nanocrystal bionanocomposites. Comp. Sci. Techn. 88 (2013) 39–47.

[7] ASTM D 4274-05. Standard Test Methods for Testing Polyurethane Raw Materials: Determination of Hydroxyl Numbers of Polyols. Test Method A (Dic 2010).
[8] A. Saralegi, L. Rueda, B. Fernández-d'Arlas, I. Mondragon, A. Eceiza, M.A. Corcuera. Thermoplastic polyurethanes from renewable resources: effect of soft segment chemical structure and molecular weight on morphology and final properties. Polym. Int. 62 (2013) 106–115.
[9] A.T. Lorenzo, M.L. Arnal, J. Albuerne , A.J. Müller. DSC isothermal polymer crystallization kinetics measurements and the use of the Avrami equation to fit the data: Guidelines to avoid common problems. Polym. Test. 26 (2007) 222–231.
[10] A.J. Müller, R.M. Michell, R.A. Pérez, A.T. Lorenzo. Successive Self-nucleation and Annealing (SSA): Correct design of thermal protocol and applications. Eur. Polym. J. 65 (2015) 132-154.
[11] B. Fernández-d'Arlas, A. Eceiza. Structure–Property Relationship in High Urethane Density Polyurethanes. J. Polym. Sci. Polym. Phys. 54 (2015) 739-746.
[12] F. Castro (2012). Síntesis y caracterización de poliuretanos termoplásticos basados en policarbonato dioles. Relación estructura/propiedades Valencia. Trabajo de Grado Doctoral (publicado on-line). Facultad de Química Universidad de Valencia, Valencia, España.
[13] A. Achilleas (2012). The role of the chain extender on the phase behaviour and morphology of high hard block content thermoplastic polyurethanes: Thermodynamics-Structures-Properties. Manchester. Trabajo de Grado Doctoral no publicado. Universidad de Manchester. United Kingdom.
[14] L. Rueda, B. Fernandez-d'Arlas, A. Tercjak, R. Greus, I. Mondragon, A. Eceiza. Synthesis and microstructure–mechanical property relationships of segmented polyurethanes based on a PCL–PTHF–PCL block copolymer as soft segment. Polym J. 45 (2009) 2096-2109.
[15] I. Yilgor, E. Yilgor, G. Wilkes. Critical parameters in designing segmented polyurethanes and the effect on morphology and properties: A comprehensive Review. Polymer 58 (2015) A1-A36.
[16] B. Fernández-d'Arlas, M.A. Corcuera, A. Eceiza. Caracterización estructural de poliuretanos segmentados elastoméricos bajo deformación uniaxial. An. Quím. 111 (2015) 83-91.
[17] L. Mandelkern. Crystallization of polymers. Equilibrium concepts. vol. 1. Cambridge: Cambridge University Press; 2002.
[18] R.S. Waletzko, L.T. Korley, B.D. pate, E.L. Thomas, P.T. Hammond. Role of Increased Crystallinity in Deformation-Induced Structure of Segmented Thermoplastic Polyurethane Elastomers with PEO and PEO-PPO-PEO Soft Segments and HDI Hard Segments. Macromolecules, 42 (2009) 2041-2053.
[19] U. Gedde, Polymer Physics, Chapman and Hall, London, 1995.
[20] B. Fernández-d'Arlas, R.P. Baumann, E. Pöselt, A.J. Müller. Influence of composition on the isothermal crystallisation of segmented thermoplastic polyurethanes. Cryst. Eng. Comm. 19 (2017) 4720-4733.

[21] M.L. Auad, V.S. Contos, S. Nutt, M.I. Aranguren, N.E. Marcovich, Characterization of nanocellulose-reinforces shape memory polyurethanes, Polym. Int. 57 (2008) 651–659.

[22] A. Kolmogorov, К статистической теории кристаллизации Металлов, Akad. Nauk SSSR, Izv., Ser. Mat. 1 (1937) 355.

[23] M. Avrami, Kinetics of phase change. II transformation-time relations for random distribution of nuclei, J. Chem. Phys. 8 (1940) 212.

[24] G. Strobl, A multiphase model describing polymer crystallization and melting, in: G. Reiter, G.R. Strobl (Eds.), Progress in Understanding of Polymer Crystallization, Lecture Notes in Physics, vol. 714, Springer-Verlag, Berlin, 2007, pp. 481–502.

[25] V. Pistor, D. de conto, F. Gustavo Ornaghi, A. Jos´e Zattera, Microstructure and crystallization kinetics of polyurethane thermoplastics containing trisilanol isobutyl POSS, J. NanoMat. (2012) 1–8. Article ID 283031.

[26] B. Fillon, J.C. Wittmann, B. Lotz, A. Thierry, Self-nucleation and recrystallization of isotactic polypropylene (α phase) investigated by differential scanning calorimetry, J. Polym. Sci., Part B: Polym. Phys. 31 (1993) 1383–1393.

[27] A.J. Müller, M.L. Arnal, Thermal fractionation of polymers, Prog. Polym. Sci. 30 (2005) 559–603.